

Validation of an Extended Kinetic Model of Free-Radical *N*-Vinylpyrrolidone Polymerization

Stefan Welzel,* Jule Burmeister, Oliver Höppchen, and Ulrich Nieken

To predict the polymer properties produced by free-radical polymerization of *N*-vinylpyrrolidone (NVP) in aqueous solution a detailed kinetic model has been developed. The kinetic model allows to calculate the chain length distribution, the number of branching points, and the number of terminal double bonds (TDB). The latter is accounted for since TDBs are a precondition for branching. While monomer conversion can be predicted sufficiently using independently determined rate constants for propagation and termination, here the predictions of structural properties by a newly developed extended kinetic model to experimental findings are compared. Polymer produced in a continuous stirred tank reactor is analyzed by gel permeation chromatography (GPC), field flow fractionation (FFF), and high-pressure liquid chromatography (HPLC).

1. Introduction

The production of specialty polymers such as polyvinylpyrrolidone (PVP) usually takes place in batch or semi-batch reactors due to a high degree of operational flexibility. To intensify the production process, continuous production is preferable due to higher energy efficiency and constant polymer properties. A serious problem in continuous operation of tubular reactors equipped with static mixing elements is the formation of fouling deposits, which grows up and subsequently leads to blocking of the reactor and shutdown. Side reactions leading to high molecular weight and branched polymer molecules are considered to be a prerequisite for fouling. Local back-mixing and stagnant flow, which occur at static mixing elements, lead to locally increased residence times and enhance the formation of a polymer network.^[1–7] Various measurement techniques have already

been evaluated for measuring or quantifying fouling in continuous reactors.^[8–11] One way to avoid or reduce fouling in microreactors is the choice of suitable coatings.^[4,12,13]


Fouling may also be reduced by a suitable choice of operation conditions and mixer geometry using a kinetic model,^[2,14] which predicts the microstructure of the resulting polymers. The reaction mechanism of the radical polymerization of NVP in aqueous solutions has been studied in several publications. The rate coefficients of propagation,^[15,16] termination,^[17] and transfer to monomer^[1,18] were determined by independent methods. The formation of terminal double bonds (TDB) by transfer to monomer was identified by Hellmund^[19]

using density functional theory (DFT) calculations. In order to model the number of TDBs Zander et al.^[20] extended the kinetic model and determined parameters for the propagation of terminal double bonds and the initiator efficiency to match the monomer conversion and the mass averaged molecular weight in a CSTR reactor. In a recently published paper,^[21] the kinetic model of Zander et al.^[20] was further extended and a one-dimensional model for chain length distribution and number of branching points (BP) was derived. Therefore, a zero dimensional TDB moment model and the branching point model were combined to determine the polymer microstructure (chain length distribution, number of BP, and TDB as a function of chain length) during transient operation of a reactor.^[21] For convenience we briefly summarize the model in this work and refer to ref. [21] for a more detailed information.

In the following, the predictions of the newly developed kinetic model and the corresponding set of parameters will be compared to experimental data. Polymerizations in a stirred tank reactor were carried out varying residence times and monomer concentrations. During transition to steady-state samples were taken and analyzed by gel permeation chromatography (GPC), field flow fractionation (FFF), and high-pressure liquid chromatography (HPLC). Molecular weight averages, monomer conversion, molecular weight distributions and branching points are compared to model predictions.

S. Welzel, J. Burmeister, U. Nieken
Universität Stuttgart
Institut für Chemische Verfahrenstechnik
Böblinger Str. 78, 70199 Stuttgart, Germany
E-mail: stefan.welzel@icvt.uni-stuttgart.de

O. Höppchen
BASF SE
Carl-Bosch-Strasse 38, 67056 Ludwigshafen, Germany

 The ORCID identification number(s) for the author(s) of this article can be found under <https://doi.org/10.1002/mren.202200075>

© 2023 The Authors. Macromolecular Reaction Engineering published by Wiley-VCH GmbH. This is an open access article under the terms of the Creative Commons Attribution License, which permits use, distribution and reproduction in any medium, provided the original work is properly cited.

DOI: 10.1002/mren.202200075

2. Experimental Section

2.1. Chemicals

BASF SE provided *N*-vinylpyrrolidone that had been stabilized with 0.5% NaOH and was then purified by distillation under

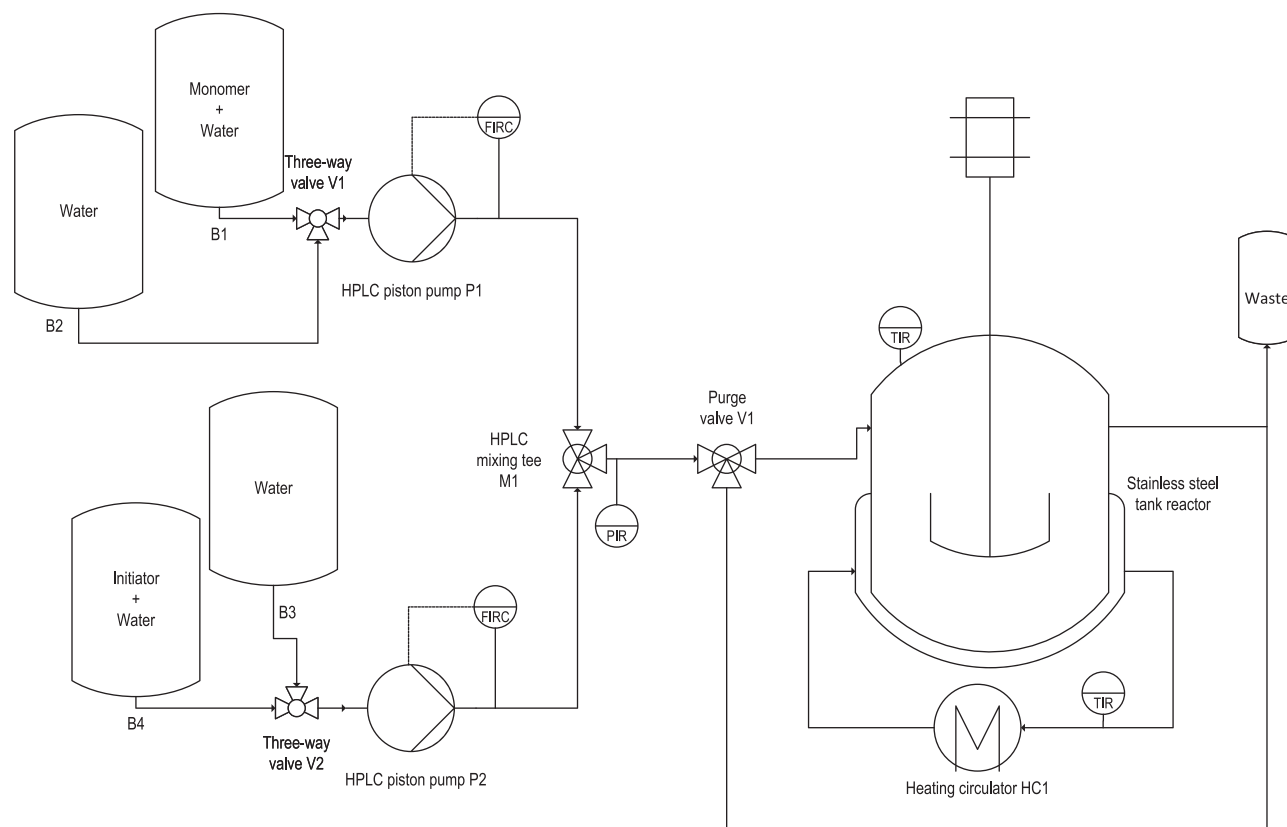


Figure 1. Simplified flow sheet of the setup for CSTR experiments.

vacuum to eliminate the stabilizer and high-molecular components just before the experiments. The initiator (V-50, Wako Chemicals) was used as given after being kept in the refrigerator. As a solvent, deionized water has been employed.

2.2. Experiments

Figure 1 shows a simplified flow sheet of the setup for the tank reactor experiments. The CSTR experiments were carried out isothermally at $T = 85^\circ\text{C}$ in a 650 mL Juchheim stirred tank reactor made of stainless steel. A mixture of monomer and solvent was prepared for one storage container, and the initiator, which had been dissolved in the solvent, was prepared for the other. Both containers were degassed under vacuum. Throughout the entire experiment, the storage container was flushed by argon to prevent oxygen from entering. Two Knauer HPLC piston pumps were used to pump the feed streams, and Bronkhorst Coriolis mass flow meters and PI controllers were used to control the flow rates. Before entering the reactor, the feed streams from both tanks were mixed in a 1:1 ratio using a static T-piece with 0.5 mm thru-holes and a 10 m frit in the center port.

2.3. Analytical Setups

Monomer conversion was determined by HPLC measurements using an Agilent 1260 series setup, a mixture of water and ace-

tonitrile (90:10) as an eluent at 0.5 mL min^{-1} flow rate. The injection volume was $3\text{ }\mu\text{L}$. A Poroshell 120EC-C18 column was used for separation, UV adsorption was measured at 235 nm. The results of three injections were averaged. Molecular weight averages and distributions as well as the radius of gyration were determined from GPC on a setup delivered by PSS (Polymer Standard Service, Mainz, Germany) using DMAc with 5 g L^{-1} LiBr as eluent at 0.8 mL min^{-1} . For separation a column set containing a $100\text{ }\text{\AA}$ column and two columns with $100\text{ }000\text{ }\text{\AA}$ pore size (GRAM ultrahigh columns set) have been used. As a concentration sensitive detector, the refractive index was measured by an Agilent 1260 Infinity II detector. The PSS SLD7100 multi angle lights scattering detector was used as a molar sensitive detector. Combining both signals allow to obtain absolute molecular weight averages and distributions. The data has been recorded using the WinGPC software. Since it was not possible to carry out structural analysis with WinGPC due to non-adjustable filters, the raw data of the detector was processed by a self-written Matlab code. The weight average molecular weight was directly calculated from the detector data. To obtain the molecular weight distributions, a linear approximation of the measured calibration curve was used where only molecular weights above 100 kg mol^{-1} were considered. Since the molecular weight averages and distributions as well as the conformation plot are strongly influenced by the anchoring effect,^[22] which means that parts of large branched polymers can behave as independent, enter pores, and anchor the entire molecules. Those are delayed and elute at higher elution volumes than their corresponding hydrodynamic volume. For

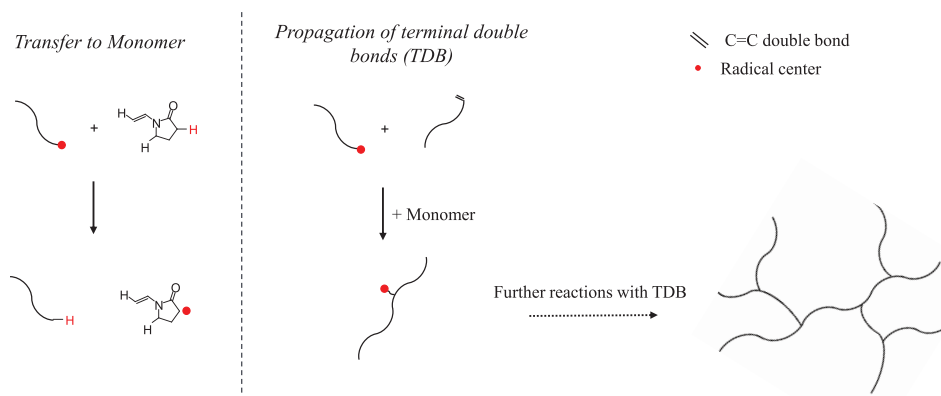


Figure 2. Reaction scheme of the side reactions “transfer to monomer” and “propagation of terminal double bonds.”

Table 1. Set of reactions for the polymerization of *N*-vinylpyrrolidone in aqueous solution with the chain length (n, m), the number of terminal double bonds (i, j) and the number of branching points (k, l).^[19]

Initiator dissociation/Initiation	$I_2 \xrightarrow{k_d} 2f_d I + M \xrightarrow{k_p} R_{1,0,0}$
Propagation	$R_{n,i,k} + M \xrightarrow{k_p} R_{n+1,i,k}$
Termination by recombination	$R_{n,i,k} + R_{m,j,l} \xrightarrow{k_{t,c}} P_{n+m,i+j,k+l}$
Transfer to monomer	$R_{n,i,k} + M \xrightarrow{k_{tr,M}} P_{n,i,k} + R_{1,1,0}$
Propagation of terminal double bonds	$R_{n,i,k} + P_{m,j,l} \xrightarrow{j \cdot k_{p,TDB}} R_{n+m,i+j-1,k+l+1}$

comparison the samples were additionally measured using FFF. For this, the Asymmetrical Flow Field-Flow Fractionation (AF4) system (Eclipse separation system AF4, Wyatt Technology, USA) with a trapezoidal channel with a nominal thickness of 350 μm (Spacer W350 μm , Wyatt Technology, USA) was used. The channel was equipped with a membrane of regenerated cellulose with 10 kDa cutoff (PLGC, Reg. Cellulose 10 kDa, Millipore, USA). The AF4 was coupled with a UV detector (DAD 1290 Infinity II, Agilent Technologies), a multi-angle light scattering detector (MALS, Dawn Heleos-II, Wyatt Technology, USA), and a differential refractive index (dRI) detector (Optilab T-rEX, Wyatt Technology, USA). The AF4 data were analyzed using Astra software, version 7.3 (Wyatt Technology, USA). A refractive index of PVP in water of $dn/dc = 0.173 \text{ mL g}^{-1}$ was used to calculate the molar mass.

2.4. Reaction Scheme

The established reaction scheme for the radical polymerization of *N*-vinylpyrrolidone was extended for side reactions in ref. [19] and is summarized in Table 1. The formation of long chains and branching is attributed to transfer to monomer and subsequent propagation of terminal double bonds. Rate parameters for these steps have been taken from literature and a fit of conversion and molecular weight measured in CSTR experiments. The dead species are denoted as P , and the living species as R . Three different property coordinates are accounted for: chain length (n, m),

number of terminal double bonds (i, j), and number of branching points (k, l). The transfer to monomer reaction generates terminal double bonds (TDB). By subsequent propagation of TDB's branched polymer chains are originated. These side reactions are depicted schematically in Figure 2. For detailed molecular structure refer to ref. [21].

The rate constants together with the corresponding literature references are listed in Table 2.

2.5. Simulations

The kinetic model, detailed in ref. [21] allows the calculation of conversion, the molecular weight distributions, and the moments of the branching point distribution as a function of chain length. The kinetic mechanism was reduced to a single coordinate in property space and integrated in the software package Predici. The procedure of model reduction is detailed in ref. [21] and briefly summarized below for convenience.

The full set of reactions listed in Table 1 spans three dimensions in property space, with coordinates chain length, terminal double bonds (TDB), and branching points (BP). Rigorous simulations with three property coordinates are practically infeasible. Therefore, the problem needs to be reduced into 1D problems along a single property coordinate. The property coordinate of TDB was reduced using a linear correlation between the average number of TDB's $p(m)$ and the chain length m (Equation (1)).

$$p(m) = A \cdot m + B \quad (1)$$

Parameters of this relation (slope (A) and axis intercept (B)) can be calculated simultaneously from a computationally cheap moment model.^[20] The resulting two-dimensional model (chain length, branching points) can be further reduced by calculation of the moments of the branching points. The K th resp. L th branching moments are defined in Equation (2) for living chains and in Equation (3) for dead chains respectively:

$$\phi_n^K = \sum_{k=0}^{\infty} k^K R_{n,k} \quad (2)$$

$$\Psi_m^L = \sum_{l=0}^{\infty} l^L P_{m,l} \quad (3)$$

Table 2. Kinetic coefficients for the reaction system of *N*-vinylpyrrolidone.

Kinetic coefficients	
$k_d/s^{-1} = 9.17 \times 10^{14} \exp(\frac{-1.49 \times 10^4}{(T/K)})$	[18]
$\frac{k_p}{k_{p,max}} = 0.36 + 0.64 \exp(-9.2 w_{NVP}) - 0.31 w_{NVP}$	[15]
with	
$\frac{k_{p,max}}{L \text{ mol}^{-1} s^{-1}} = 2.57 \times 10^7 \exp(\frac{2.12 \times 10^3}{(T/K)})$	
$\frac{k_t}{L \text{ mol}^{-1} s^{-1}} = (\frac{1}{k_{SD}} + \frac{\eta}{k_{TD}})^{-1} + k_{RD}$	[17]
with	
$\frac{k_{SD}(p)}{L \text{ mol}^{-1} s^{-1}} = (4.87 \times 10^7 \exp(-\frac{w_{NVP}}{0.29}) + 5.47 \times 10^6) \cdot \exp(-5.61 \times 10^{-4} (\frac{p}{bar} - 2000))$	
$k_{TD} = 31 k_{SD}$	
$\eta = \exp(14.75 w_{PVP})$	
$k_{RD} = 140 w_{NVP} k_p$	
with the mass fraction w_{NVP} for NVP resp. w_{PVP} for PVP and the viscosity η .	
$\frac{k_{tr,m}}{k_p} = 6 \cdot 10^{-4}$	[18]
$\frac{k_{p,TDB}}{L \text{ mol}^{-1} s^{-1}} = 3300$	[20]
$f_d = 0.7$	[18]

Table 3. Operational parameters used in experiments if not stated otherwise.

Feed	
Monomer weight fraction w_{NVP}^+	0.2/0.1
Initiator weight fraction $w_{I_2}^+$	0.0002
Solvent weight fraction $w_{H_2O}^+$	$1 - w_{NVP}^+ - w_{I_2}^+$
Feed rate \dot{m}_F [g min ⁻¹] resp. average residence time $\bar{\tau}$ [h]	13.94/4.7/2.35 resp. 0.75/2.25/4.5
Initial conditions in reactor	
Solvent weight fraction $w_{H_2O}^0$	1
Reactor temperature T_R [°C]	85
Reactor volume V_R [mL]	650
$\rho_{H_2O}(85^\circ\text{C})$ [kg m ⁻³]	959[18]
$\rho_{NVP}(85^\circ\text{C})$ [kg m ⁻³]	989[18]

Finally, one obtains a one-dimensional model: the chain length distribution of dead and living polymers and the moments of the branching point distribution as a function of chain length. Reduction of property space from three to one property coordinate has already been validated by comparison to a computationally expensive class model in ref. [21].

3. Results

To test the predictive capability of the kinetic model, simulations will be compared to experimental data subsequently. Unless otherwise stated, the process parameters correspond to the reference case, which is given in Table 3.

3.1. Molecular Weight Averages and Monomer Conversion

In Figure 3A–D, the simulations of the average molecular weight and the monomer conversion are compared to experimental results. Samples were taken at different times after startup and normalized by average residence time. The molecular weight M was

determined by GPC resp. FFF, which were coupled with concentration and molar mass sensitive detectors. The molecular weight averages have been calculated using Equation (4)

$$\bar{M}_w = \frac{\sum_i c_i M_i}{\sum_i c_i} \quad (4)$$

with the mass concentration c_i , the corresponding molecular weights M_i and i indicates the i^{th} elution volume slice.^[22] By using high performance liquid chromatography (HPLC) monomer conversion is monitored along reaction time. The sample material is separated according to the polarity of the components and then analyzed with a UV detector. Thereby, the concentration of the sample component, in this case the monomer concentration, can be determined. From the feed monomer weight fraction w_M^+ and the monomer weight fraction of the sample w_M , the conversion in a CSTR can be calculated by Equation (5).

$$X_M = \frac{w_M^+ - w_M}{w_M^+} \quad (5)$$

Figure 3A shows the plot of \bar{M}_w for a CSTR reactor at different average residence times and a monomer weight fraction of 20 wt% in the feed. With increasing residence time, the average molecular weight increases. In general, the experimental data can be well reproduced by the simulations.

Monomer conversions versus reduced reaction times are plotted in Figure 3B. At higher average residence time, monomer conversion increases initially fast and quickly approaches the steady-state value. Predicted conversions are in good agreement with measurements, whereby the simulations slightly overestimate monomer conversion.

\bar{M}_w for a CSTR at different average residence times and a monomer concentration of 10 wt% is plotted in Figure 3C. Again, the clear trend between \bar{M}_w and residence time is obvious.

The corresponding monomer conversions plotted in Figure 3D also show good agreement between simulations and the experiments. Like for feed concentration of 20 wt%, there is a slight overestimation by model predictions.

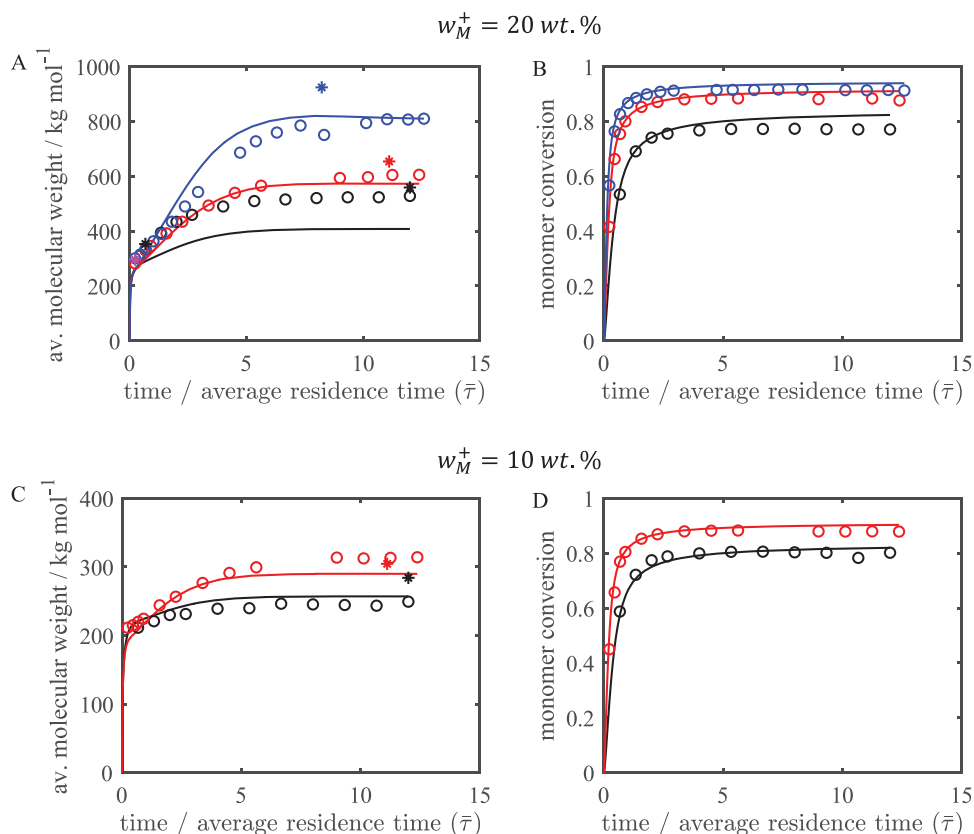


Figure 3. Comparison of the evolution of the average molecular weight and monomer conversion for simulations (lines) and experiments (GPC—circle; FFF—star) at different average residence times: black—0.75 h; red—2.25 h; blue—4.5 h. A,B) $w_M^+ = 20$ wt%; C,D) $w_M^+ = 10$ wt%.

In general, the predictions of simulations and experimental data show good agreement with respect to the molecular weight averages and the monomer conversion except for $w_{NVP}^+ = 20$ wt% and $\bar{\tau} = 0.75$ h. At low reaction times average molecular weight and the monomer conversion increases sharply. Then the curves slowly approach the steady state. It is evident, that the average steady state molecular weight from GPC data for a monomer feed concentration of 20 wt% is slightly underestimated at low residence times. The experimental molecular weight for a monomer feed concentration of 10 wt% fit better to the simulations for both average residence times. The reason for this may be that $k_{p,TDB}$ is taken as constant although the propagation of TDB is a reaction between two macromolecules and might be diffusion-limited, which means that the reaction rate is affected by the size of the polymer chains. It can be expected that the coefficient would decrease with higher polymer content and a corresponding increase in viscosity. This is especially true for high average residence times and high monomer feed concentrations. Therefore, for smaller molecules (10 wt% monomer feed concentration) the diffusion limitation does not have such a strong impact. The results of the FFF for all residence times are underestimated by the simulations. The experimental results of GPC fit better in total to the simulations because the value for $k_{p,TDB}$ was adjusted to the molecular weights of GPC measurements in a previous work.^[20] Since only a few samples were investigated with FFF, it is not possible to obtain a clear tendency.

3.2. Molecular Weight Distribution at Steady State

As mentioned before, measurements with concentration and molar mass sensitive detectors can determine the mass concentration c_i and the weight-average molecular weight \bar{M}_w as a function of time or the elution volume V_i^{elu} . The weight fractions w_i at the corresponding elution volumes^[22] and can be calculated by Equation (6).

$$w(V_i^{elu}) = \frac{c_i}{\sum_i c_i} \quad (6)$$

Since the data provided by the detectors are dependent on the selected separation system (GPC or FFF), Equation (6) needs to be converted to a molecular weight-dependent function $w(M_i)$ or $w(\log M_i)$. At this point, the usual logarithmic calibration curve $\log M(V_i^{elu})$ is used and the relationship depicted in Equation (7) between the two distributions is obtained.^[22,23]

$$w(\log M_i) = \pm w(V_i^{elu}) \frac{dV_i^{elu}}{d \log M_i} \quad (7)$$

The choice of sign depends on the chosen separation method. For GPC data the sign must be chosen negative, since the molecular weight decreases with increasing elution volume.^[23] For the

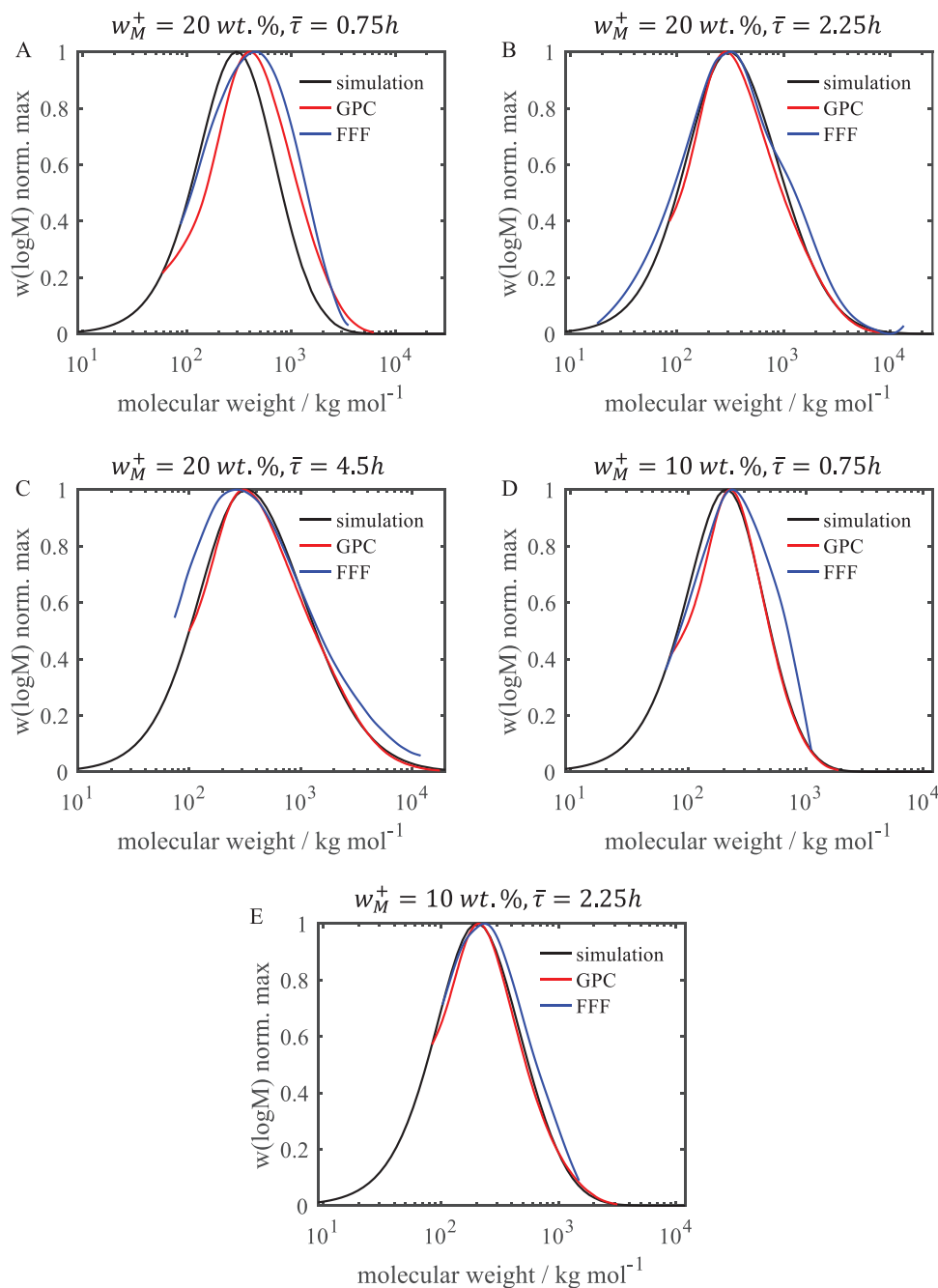


Figure 4. Comparison of the normalized GPC distribution from experiments and simulations at different average residence times and monomer feed concentrations. A) $w_M^+ = 20$ wt% and $\bar{\tau} = 0.75$ h; B) $w_M^+ = 20$ wt% and $\bar{\tau} = 2.25$ h; C) $w_M^+ = 20$ wt% and $\bar{\tau} = 4.5$ h; D) $w_M^+ = 10$ wt% and $\bar{\tau} = 0.75$ h; E) $w_M^+ = 10$ wt% and $\bar{\tau} = 2.25$ h.

evaluation of FFF sign must be positive, as the molecular weight increases with increasing elution volume.

The last sampling time (12× average residence times) was taken as the steady state for the average molecular weight for the experiments, which, according to Figure 3A,C, did not change after 10 average residence times.

Figure 4A shows the comparison of the normalized GPC distributions of the CSTR experiment with the simulation at an aver-

age residence time of $\bar{\tau} = 0.75$ h and a monomer weight fraction of 20 wt% in the feed. For the FFF result, there is a broadening of the peak compared to the simulations and the results of the GPC. The simulation here slightly underestimates the molecular weight and for this reason the complete distribution is slightly shifted to smaller molecular weights.

The comparison for the residence time of 2.25 h and a monomer weight fraction of 20 wt% in the feed is shown in

Figure 4B. The GPC and FFF results are in better agreement with the simulation results than the results obtained with an average residence time of 0.75 h.

Figure 4C shows the distributions at a residence time of 4.5 h and a monomer feed concentration 20 wt%. The GPC results are in very good agreement with the simulation. However, there is a widespread peak in the FFF results. In general, the molar mass distributions between simulation and experiment differ for 20 wt% monomer feed concentration at low residence time of 0.75 h and better agree for longer residence times. Again, this can be explained by the fact that a constant parameter for $k_{p,TDB}$ is inappropriate and thus the reaction rate does not depend on the pore size.

The normalized GPC distributions at an average residence time of 0.75 h and a monomer weight fraction of 10 wt% in the feed are shown in Figure 4D. Thereby, the results of GPC show very good agreement and those of FFF are broadened for high molecular weights.

The comparison at a residence time of 2.25 h and a monomer weight fraction of 10 wt% in the feed, which is shown in Figure 4E, also shows good agreement between the experimental results both for FFF and GPC and the simulations. In contrast to the experiments at higher monomer concentration, the experimental and simulated molar mass distributions agree better for a monomer concentration of 10 wt%, since diffusion limitation is not as important for smaller molecules.

As shown in Figure 4A–E, the steady state molecular weight distribution of CSTR experiments at different residence times and monomer weight fractions in the feed can be well represented by the simulations. Furthermore, the FFF results are shifted to higher molecular weights compared to the GPC results. The reason for this is that interactions between large molecules and the gel, which is used for the separation, can occur during separation with GPC. Moreover, shear degradation of polymer molecules with a molar weight over 10^6 g mol^{-1} is possible. The figures also show that for higher residence times there is a broadening of the distribution and a shift toward higher molecular weights. This can be explained by the fact that the increased residence time results in the formation of longer chains and increased branching.

3.3. Characterization of Branching Points

For the characterization of polymers, the radius of gyration R_g is often used, since this can provide information about the polymer size independent of the molecular structures.^[23] As mentioned in Section 2.3 the GPC and FFF were coupled with a molar mass sensitive and concentration sensitive detector. The MALS detectors based on elastic light scattering from particles were used as the molar mass sensor. If a laser beam with the specific wavelength λ_L is directed onto the sample material, the light scatters with different scattering intensities. The intensities and the corresponding light scattering angles are detected and averaged over time. From the measured data, the radius of gyration can be determined. For this, the Berry plot (Equation (8))

$$\sqrt{\frac{K^*c}{R_\theta}} = \frac{1}{M_w} + \frac{16\pi^2 R_g^2}{3M_w \lambda_L^2} \cdot \sin^2\left(\frac{\theta}{2}\right) \quad (8)$$

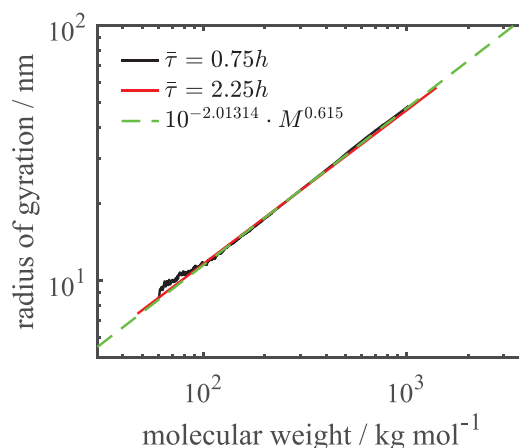


Figure 5. Comparison of the conformation plots from CSTR experiments with different average residence times at early operating times. The green dashed line is the power law fit, which is used as a linear reference.

with is the Rayleigh ratio R_θ , the optical constant of the detector K^* , the specific wavelength λ_L^2 and the scattering angle θ is plotted against $\sin^2(\frac{\theta}{2})$ and fitted by a polynomial function.^[22]

The radius of gyration can then be calculated from the slope. To calculate the branching points of a polymer, the branching ratio

$$g = \frac{R_{gbr}^2}{R_{glin}^2} \quad (9)$$

was first determined, in which the index br and lin denote the squared radius of gyration of a branched resp. a linear chain with the same molecular weight.^[22]

The conformation plots of samples from CSTR experiments analyzed with FFF for different average residence times are shown in Figure 5. Samples were taken at early operating times with polymer contents around 5 wt% and monomer conversions less than 50%. The plots coincide for all residence times. Therefore, the molecular structure of the polymers of the samples should be identical, which means short and unbranched chains. A relation can be approximated with a power law^[22] by Equation (10).

$$\left\langle R_g^2 \right\rangle_{lin} = 10^{(-2.01314)} \cdot M^{0.615} \quad (10)$$

The number of branches BP was calculated assuming for trifunctional branches (since during polymerization a monomer can form three bonds to further monomers^[22]) by

$$g = \left[\left(1 + \frac{BP}{7} \right)^{0.5} + \frac{4BP}{9\pi} \right]^{-0.5} \quad (11)$$

In the following, the experimental and simulated data are compared with respect to the branching points.

Figure 6A–F shows the number of BP as well as the number of BP per 1000 repeat units (RU) for CSTR experiments along the molecular weight for different residence times and different monomer weight fractions in the feed.

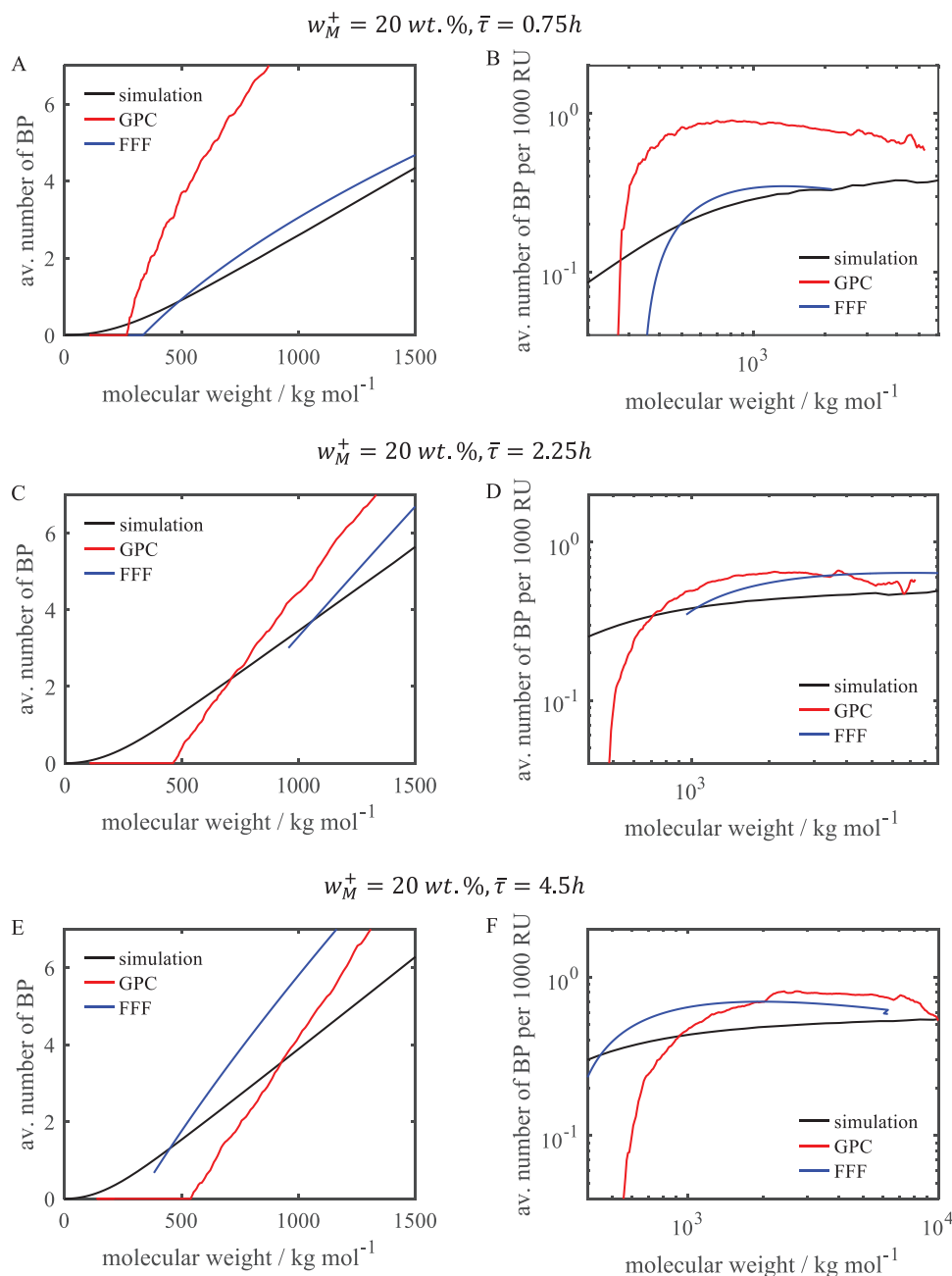


Figure 6. Comparison of the number of branching points and the number of branching points per 1000 RU from experiments and simulations at different average residence times and $w_M^+ = 20$ wt%. A,B) $\bar{\tau} = 0.75$ h; C,D) $\bar{\tau} = 2.25$ h; E,F) $\bar{\tau} = 4.5$ h.

At a monomer weight fraction of 20 wt% in the feed, the simulations are in good agreement with the experimental data from GPC and FFF. The results for an average residence time of $\tau = 0.75$ h is shown in Figure 6A with the average number of branching points over the molecular weight and in Figure 6B the average number of branching points per 1000 repeat units. Here, the simulation results agree better with the FFF results than with the GPC results. Furthermore, no branching points can be detected by the GPC and FFF at very small molecular weights. The reason for this is the instrument design, which cannot reliably measure particles sizes <10 nm with light scattering.

Figure 6C,D shows the comparison at an average residence time of 2.25 h. The experimental results of the GPC and FFF are in good agreement for higher molecular weights. It can also be seen that there is a higher branching formation compared to the residence time of 0.75 h.

The comparison at a residence time of 4.5 h is shown in Figure 6E,F. The results conducted by the experiments can be represented by the simulations reasonably well. The simulation slightly underestimates the number of BP for higher molecular weights. Compared to the lower residence times of 0.75 and 2.25 h, there is a higher formation of branching points. Thus, for

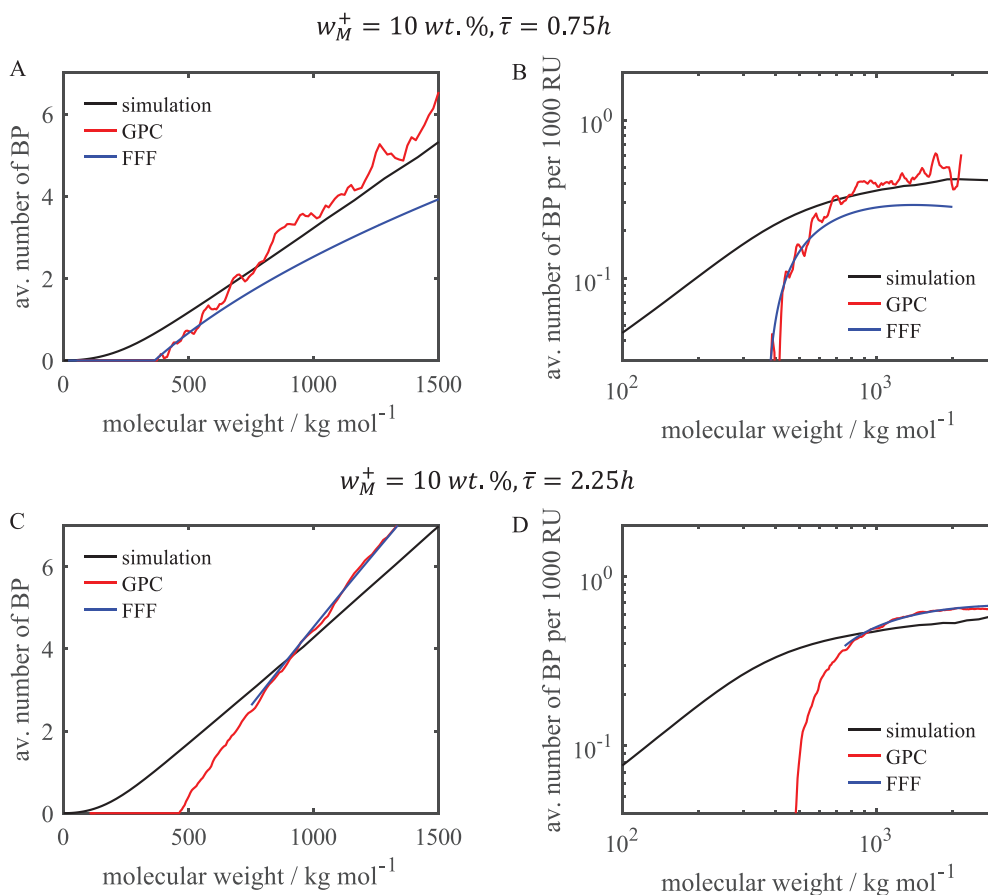


Figure 7. Comparison of the number of branching points and the number of branching points per 1000 RU from experiments and simulations at different average residence times and $w_M^+ = 10 \text{ wt.}\%$. A,B) $\bar{\tau} = 0.75 \text{ h}$; C,D) $\bar{\tau} = 2.25 \text{ h}$.

higher residence times, the increase in number of branches is higher than predicted by the model. The reason for this is that parameter $k_{p,TDB}$ is treated as a constant parameter, which is slightly underestimated in this case, because the increased monomer conversion with higher average residence times, leads to an increase of the probability of side reactions, such as the transfer to monomer and propagation of terminal double bonds.

At a monomer weight fraction of 10 wt% in the feed the experimental data for a residence time of 0.75 h, in **Figure 7A,B** can be well described by the simulations.

Figure 7C,D shows the comparison at a residence time of 2.25 h and a monomer weight fraction of 10 wt% in the feed. In comparison with the residence time of 0.75 h, there is also an increased branching formation. This is again due to higher monomer conversion, which leads to an increase of the side reactions and thus to branching.

It has been shown that the experimental trends can be well covered by the simulations at NVP feed concentrations between 10 and 20 wt%. In most cases the number of branches is underestimated by the simulations. The presented results from CSTR experiments should only be interpreted qualitatively, since the description of the linear reference sample by a power law function relies on only two linear samples. An approximation with a higher number of linear samples could minimize the error.

Moreover, due to the non-ideal separation of branched samples at low molecular weights, linear extrapolation was used for the GPC data which leads to additional errors.

4. Conclusion

To validate the kinetic model, simulated data were compared with experimental results obtained from CSTR experiments with NVP feed concentrations of 10 and 20 wt%. The analysis of the polymer samples was carried out using gel permeation chromatography, field flow fractionation and high pressure liquid chromatography. In general, the simulations show good agreement with the experimental data with respect to the molecular weight averages, molecular weight distributions as well as monomer conversion and number of branching points. It was shown that the average number of branching points increases steeply for higher residence times. This trend could be observed both in simulations and experimental data collected by GPC resp. FFF. Additionally, the monomer content in the feed stream influences the formation of branched polymers. A lower monomer concentration leads to a higher number of branching points.

However, the separation of polymer molecules by GPC may lead to a distortion of the results due to anchoring effects. Another source of uncertainty of the experimental data with respect

to the branching points are the assumptions made for the calculation of branching. Assuming a constant $k_{p,TDB}$ could be the reason, although the propagation of TDB may be diffusion-limited, which means the reaction rate is affected by the size of the polymer chains.

The evolution of the molecular weight average and monomer conversion as well as molecular weight distribution can be well represented by the model. The average number of branching points also shows qualitative agreement between the model-based simulations and the experimental data. These results support the validity of the reaction mechanism and the mathematical model.

Acknowledgements

The financial support of the German Federal Ministry for Economic Affairs and Climate Action (BMWK) under grant numbers 03EN2004F and 03EN2004A (UNIS, BASF, KoPPonA 2.0) is gratefully acknowledged.

Open access funding enabled and organized by Projekt DEAL.

Conflict of Interest

The authors declare no conflict of interest.

Data Availability Statement

The data that support the findings of this study are available from the corresponding author upon reasonable request.

Keywords

branching point distribution, kinetic modelling, model validation, *N*-vinylpyrrolidone, radical polymerization, side reactions

Received: December 7, 2022

Revised: January 23, 2023

Published online: February 17, 2023

- [1] J. Urrutia, A. Peña, J. M. Asua, *Macromol. React. Eng.* **2017**, *11*, 1600043.

- [2] D. Kohlmann, M. C. Chevrel, S. Hoppe, D. Meimaroglou, D. Chapron, P. Bourson, C. Schwede, W. Loth, A. Stammer, J. Wilson, P. Ferlin, L. Falk, S. Engell, A. Durand, *Macromol. React. Eng.* **2016**, *10*, 339.
- [3] C. Bernstein, *Methoden zur Untersuchung der Belagsbildung in Chemischen Reaktoren*, Universität Hamburg, Hamburg **2017**.
- [4] C. Zander, *Fouling During Solution Polymerization in Continuously Operated Reactors*, Universität Stuttgart, Stuttgart **2021**.
- [5] S. Fries, D. M. Castañeda-Zúñiga, J. Duchateau, P. Neuteboom, C. T. Porras, M. Busch, *Macromol. Symp.* **2016**, *360*, 78.
- [6] A. Buchelli, M. L. Call, A. L. Brown, A. Bird, S. Hearn, J. Hannon, *Ind. Eng. Chem. Res.* **2005**, *44*, 1474.
- [7] M. F. Cunningham, H. K. Mahabadi, K. F. O'Driscoll, *Polym. React. Eng.* **1993**, *1*, 245.
- [8] A. Hohlen, W. Augustin, S. Scholl, *Macromol. React. Eng.* **2020**, *14*, 1900035.
- [9] A. Böttcher, J. Petri, A. Langhoff, S. Scholl, W. Augustin, A. Hohlen, D. Johannsmann, *Macromol. React. Eng.* **2022**, *16*, 2100045.
- [10] M. Osenberg, J. Forster, S. Rust, T. Fritsch, J. Tebrugge, W. Pauer, T. Musch, *Proc. IEEE Sens. IEEE, Dallas, TX, USA* **2022**, 2022-October.
- [11] B. Gieseke, B. Jäck, E. Preis, S. Jung, M. Forster, U. Scherf, C. Deibel, V. Dyakonov, *Adv. Energy Mater.* **2012**, *2*, 1477.
- [12] Y. Liu, H. Wang, Q. Liu, H. Qu, B. Liu, P. Yang, *Lab Chip* **2010**, *10*, 2887.
- [13] V. Neßlinger, S. Welzel, F. Rieker, D. Meinderink, U. Nieken, G. Grundmeier, *Macromol. React. Eng.* **2022**, *17*, 2200043.
- [14] C. P. Bokis, S. Ramanathan, J. Franjione, A. Buchelli, M. L. Call, A. L. Brown, *Ind. Eng. Chem. Res.* **2002**, *41*, 1017.
- [15] M. Stach, I. Lacík, D. Chorvát, M. Buback, P. Hesse, R. A. Hutchinson, L. Tang, I. Lacík, D. Chorvát, M. Buback, *Macromolecules* **2008**, *41*, 5174.
- [16] L. Uhelská, D. Chorvát, R. A. Hutchinson, S. Santanakrishnan, M. Buback, I. Lacík, *Macromol. Chem. Phys.* **2014**, *215*, 2327.
- [17] J. Schrooten, M. Buback, P. Hesse, R. A. Hutchinson, I. Lacík, *Macromol. Chem. Phys.* **2011**, *212*, 1400.
- [18] S. Santanakrishnan, L. Tang, R. A. Hutchinson, M. Stach, I. Lacík, J. Schrooten, P. Hesse, M. Buback, *Macromol. React. Eng.* **2010**, *4*, 499.
- [19] P. Deglmann, M. Hellmund, K. Hungenberg, U. Nieken, C. Schwede, C. Zander, *Macromol. React. Eng.* **2019**, *13*, 1900021.
- [20] C. Zander, K. D. Hungenberg, T. Schall, C. Schwede, U. Nieken, *Macromol. React. Eng.* **2020**, *14*, 2000009.
- [21] S. Welzel, C. Zander, K. Hungenberg, U. Nieken, *Macromol. React. Eng.* **2022**, *16*, 2200005.
- [22] S. Podzimek, *Light Scattering, Size Exclusion Chromatography and Asymmetric Flow Field Flow Fractionation: Powerful Tools for the Characterization of Polymers, Proteins and Nanoparticles*, John Wiley & Sons, Inc., Hoboken, NJ, USA **2011**.
- [23] M. Rubinstein, R. H. Colby, *Polymer Physics*, Oxford University Press, Oxford **2003**.